THE JOURNAL OF PHYSICAL CHEMISTRY C
A JOURNAL OF THE AMERICAN CHEMICAL SOCIETY

pubs.acs.org/JPCC

Article

Microscopic Diffusion of Atomic Hydrogen and Water in HER Catalyst MoS_2 Revealed by Neutron Scattering

Vitalii Kuznetsov, Leran Lu, Michael M. Koza, Detlef Rogalla, Varvara Foteinou, Hans-Werner Becker, Alexei Nefedov, Franziska Traeger, and Peter Fouquet*

Cite This: *J. Phys. Chem. C* 2022, 126, 21667−21680

Read Online

ACCESS | Metrics & More | Article Recommendations | Supporting Information

ABSTRACT: The design of novel and abundant catalytic materials for electrolysis is crucial for reaching carbon neutrality of the global energy system. A deliberate approach to catalyst design requires both theoretical and experimental knowledge not only of the target reactions but also of the supplementary mechanisms affecting the catalytic activity. In this study, we focus on the interplay of hydrogen mobility and reactivity in the hydrogen evolution reaction catalyst MoS_2. We have studied the diffusion of atomic hydrogen and water by means of neutron and X-ray photoelectron spectroscopies combined with classical molecular dynamics simulations. The observed interaction of water with single-crystal MoS_2 shows the possibility of intercalation within volume defects, where it can access edge sites of the material. Our surface studies also demonstrate that atomic hydrogen can be inserted into MoS_2, where it then occupies various adsorption sites, possibly favoring defect vicinities. The motion of H atoms parallel to the layers of MoS_2 is fast with $D \approx 1 \times 10^{-9}$ m^2/s at room temperature and exhibits Brownian diffusion behavior with little dependence on temperature, i.e., with a very low diffusion activation barrier.

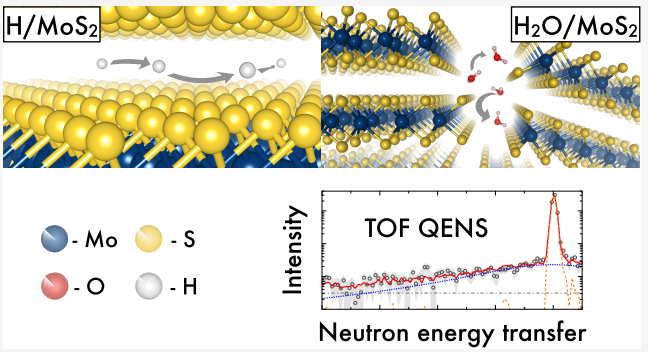

INTRODUCTION

Decarbonization of the global energy system is one of the most urgent and most complex endeavors of our time. In this context, hydrogen gas is believed to be an important energy carrier because it can be produced and subsequently converted via "green" processes. For the conversion, the use in fuel cells has already advanced to the market.[1,2]

The process of water splitting for hydrogen production seems straightforward, but it is hampered by overvoltages and hence effective catalysts are needed. To date, for the hydrogen evolution reaction (HER), platinum is the prevalent catalyst; however, its high price amounts to a significant proportion of the total costs.[3] Therefore, in recent years, extensive studies on more abundant binary compounds have been performed. Since the first work,[4] MoS_2-based catalysts have been shown to be promising substitutes for platinum.[5] The activity of this material can be increased to a level comparable to that of platinum by tailoring the number of active sites and by doping effects, which increase the bulk and interface conductivity and modify to some extent the surface chemistry.[6−9]

For the optimization of catalytic materials, it is crucial to gain physical insights into all chemical processes at the surface. This scope includes not only target reactions and side reactions but also diffusion of species on the surface or in the subsurface range. The mobility of species often is a key step in a catalytic cycle if the material does not provide a large number of reactive sites, but fast reaction on few sites followed by some form of storage of reactive species. An example of this type of reaction includes gas phase reactions of organic molecules with sulfidic catalysts, including MoS_2.[10] In the context of hydrogenation reactions, the reactivity has been linked to spillover hydrogen, i.e., hydrogen atoms diffusing away from the reactive site. Therefore, it can be concluded that also in water splitting the migration of a particular hydrogen species to a site for recombination may play an important role.

Specifically, for water electrolysis, two alternative mechanisms have been proposed,[11−15] which differ in the step of recombination to molecular hydrogen: the Heyrovsky mechanism involves the transport of a solvated proton to an adsorbed hydrogen atom, whereas the Tafel mechanism includes the recombination of two adsorbed H atoms. Density functional theory (DFT) studies and electrochemical experiments[5,11,12] indicate that the Heyrovsky mechanism is

Received: June 7, 2022
Revised: November 10, 2022
Published: December 19, 2022

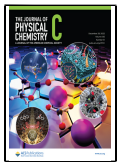

preferred. However, the diffusion of neutral atoms has also been observed.[13]

In a previous article, we studied the diffusion of hydrogen in electrochemically loaded MoS_2 samples.[16] In our study, we identified hydrogen mobility on a vast range of time and length scales as well as changes in the chemistry of MoS_2 as a function of temperature. The complexity of the processes observed, however, exposed the need for further studies that prepare the samples in different initial conditions. In particular, we found that samples loaded by electrolysis may show migration of a number of hydrogen species, and, in our experiments, H_2 molecules seemed to predominate. On the other hand, the diffusion of atomic hydrogen is of greater importance for comparison with a vast majority of numerical simulations available in the literature at the present time. Furthermore, the behavior of surface water is also a crucial aspect in proton delivery and exchange near the active sites. Hence, in the current study, we extend our investigation to MoS_2 samples that were loaded via either hydrogen atom beams or through exposure to purified water. In addition, we have enlarged the scope of our methods, which now include molecular dynamics (MD) simulations providing essential complementary arguments for the interpretation of the experimental results.

EXPERIMENTAL SECTION

Sample Preparation. Commercial MoS_2 polycrystals with a thickness of around 0.2 mm and area varying from 5 to 50 mm^2, obtained from PLANO (PLANO GmbH Wetzlar, Germany, distributor of SPI), were used as target materials for hydrogen dosage. They possess a layered, hexagonal $P6_3/mmc$ structure, with stacked S−Mo−S trilayers separated by approximately 6 Å and held together by van der Waals interactions. The crystals were divided into two sets. One set was loaded with H atoms via atom beam bombardment, while the other one was with H_2O via soaking in purified water (Milli-Q, Merck KGaA, Darmstadt, Germany). In the following, we will call the former samples H/MoS_2 and the latter H_2O/MoS_2. The experimental setup for the atom beam loading is depicted in Figure S1 of the Supporting Information.

For preparing the atom beam-loaded samples, a flat sample is first mounted onto a tantalum plate and fixed with tantalum stripes. Then, the sample holder is inserted into a chamber, which is subsequently vacuum-pumped until a pressure in the range of 10^{-8} mbar is reached. Afterward, the sample is degased several times at temperatures from 750 to 850 K to eliminate any hydrogen remaining from previous experiments. When the sample temperature returns to 300 K, the hydrogen loading commences. The valve to the H_2 source is partially opened to create a hydrogen gas flow into the chamber in a way that under constant pumping the pressure in the chamber stabilizes at $(3-5) \times 10^{-6}$ mbar. After this, the tungsten filament, placed between the H_2 source and the sample, is heated to $T \approx 1900$ K, which leads to the dissociation of a part of the H_2 molecules into atoms.[17−19] Subsequently, hydrogen atoms impinge the MoS_2 crystals and get trapped inside the material. Here, we used a loading time of 2 h. For the X-ray photoelectron spectroscopy (XPS) measurements, the crystals were prepared several days in advance, while for the neutron experiment, the crystals were loaded from one side 3 months prior to the measurements and from the other side one week in advance. Shortly before the neutron experiment, the crystals were baked for 6 h at 390 K for surface cleaning purposes. The second set of crystals was soaked in purified H_2O for several hours right before each measurement. Prior to mounting the water-loaded crystals, they were gently dried with a paper cloth to remove any excess water.

The presence of hydrogen in the H/MoS_2 samples as well as the absence of possibly intercalated water in H_2O/MoS_2 have been proven by a hydrogen depth profile via nuclear resonant reaction analysis (NRRA, $^{15}N + {}^1H \rightarrow {}^{12}C + \alpha + \gamma$). In situ NRRA measurements also showed no hydrogen uptake by MoS_2 under H_2 flow with the filament switched off. The experiments were performed at the NRRA beamline at RUBION, Bochum, Germany. More detailed information about the instrument and the analysis can be found elsewhere.[20]

X-ray Photoelectron Spectroscopy. X-ray photoelectron spectroscopy (XPS) is based on the photoelectric effect, i.e., electron emission from a specimen under electromagnetic radiation. In a given material, the strength of the binding energy of an electron and its corresponding atom depends on the local chemistry of the atom. By irradiating a specimen with X-rays of a known energy, $\hbar\omega$, and measuring the energy of the emitted electrons, E_{kin}, it is possible to obtain the distribution of binding energies of the emitted electrons with the following equation[21]

$$E_{bin} = \hbar\omega - E_{kin} - \phi \quad (1)$$

where ϕ is an instrument function. Any electron ejected from an atom below the outer surface of the sample material needs first to traverse several atomic layers before it can reach vacuum and be collected at the analyzer. This leads to a decrease in signal intensity from the underlying layers and, essentially, to a notion of effective analysis depth, which, in the case of MoS_2, can be approximated to slightly more than one S−Mo−S layer.[22,23]

The XPS measurements were performed on the HE-SGM station at the BESSY II synchrotron, Helmholtz-Zentrum Berlin (HZB), Germany, which possesses a Scienta R3000 XPS analyzer and a photon beam size of 2×0.2 mm^2. The pass energy for the collected electrons was set to 50 eV to reduce the background. The excitation energies of the incoming beam for H/MoS_2 were set to 750, 500, 450, and 380 eV for the oxygen, carbon, molybdenum, and sulfur lines, respectively, while for H_2O/MoS_2, it was fixed at 700 eV for oxygen and to 350 eV for all of the other elements. We note that a difference in excitation energies may slightly alter the resulting intensities of elemental lines due to a variation in the analysis depth in the case of H_2O/MoS_2; however, the effect is minor in our case. To monitor the changes in surface chemistry upon hydrogen desorption, the samples were exposed to temperature treatment in situ. Both specimens were heated up to 550 K with the manually controlled heater ramp at ∼10 K/min, and XPS scans were conducted at several intermediate temperatures. The XPS scans could not be conducted while the samples were at elevated temperatures because the sample heating increased the chamber pressure to levels that were incompatible with the operation of the electron energy analyzer and detector. Therefore, before each scan, the system was left to rest for some time to let the pressure in the chamber return to operating values. The temperatures displayed in the graphs, therefore, represent the maximum temperature the crystal was heated to and not the temperature during the measurement. Heavy desorption from the H/MoS_2 crystal did not allow one to perform the whole treatment in one run; thus, a second run was carried out to reach 550 K. Approximately 14 h had to be

https://doi.org/10.1021/acs.jpcc.2c03848
J. Phys. Chem. C 2022, 126, 21667−21680

skipped between the first and the second heating run for H/MoS_2. This issue will be addressed later in the Results and Discussion section. The analysis of the data was performed with the help of the XPST package within Igor Pro software (WaveMetrics, Portland). The energy calibration for each sample and each temperature was conducted by referring to the corresponding adventitious C 1s line at 284.8 eV. The background was treated by means of the Shirley step model,[24] and the intensities were corrected for the atomic subshell photoionization cross sections.[25]

Time-of-Flight (TOF) Quasi-Elastic Neutron Scattering (QENS). Quasi-elastic neutron scattering is a powerful nondestructive method allowing one to investigate the properties of hydrogen diffusion within the bulk of a material. It essentially yields a time-space Fourier transform of an autocorrelation function of a moving particle,[26] and thus, it can be interpreted in terms of general models for microdiffusion.

The prepared samples H/MoS_2 and H_2O/MoS_2 were measured on the neutron time-of-flight (TOF) spectrometer IN6-SHARP at Institut Laue-Langevin (ILL), Grenoble, France.[27] The instrument operates based on a time-focusing TOF principle. For an optimal resolution-flux ratio, neutrons of wavelength λ = 5.12 Å were used. The MoS_2 crystals were placed in a flat aluminum cell, which was not vacuum-tight to allow any desorbed gases to leave the system. The sample cell was inserted into an "orange" cryofurnace[28] and positioned such that the MoS_2(0001) basal planes were parallel to the momentum transfer vector, the so-called in-plane geometry (Figure 1). This setup allows one to study the diffusion

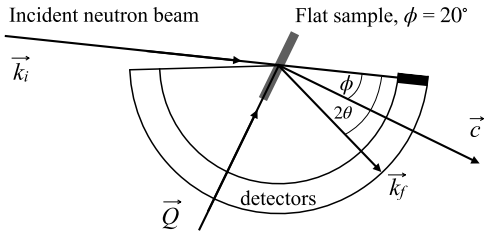

Figure 1. Basic scheme of the experimental layout of the neutron scattering experiment. The incident neutron beam with a wave vector k_i falls on a flat MoS_2 sample and is scattered at an angle 2θ with a final wave vector k_f. For a defined angle ϕ between the incident beam direction and normal to the sample's surface c, there will exist an angle 2θ for which the momentum transfer vector $\mathbf{Q} = \mathbf{k}_i - \mathbf{k}_f$ is parallel to the MoS_2 basal planes, satisfying the in-plane scattering geometry condition.

phenomena along the MoS_2 layers only. Nevertheless, the perpendicularity condition cannot, obviously, be strictly satisfied for each scattering angle simultaneously. The momentum transfer vector Q for which this condition is best fulfilled is 0.85 $Å^{-1}$. For the largest Q values used in further analysis, the ratio $Q_{\parallel}/Q$ reaches 0.8, meaning that the data at these Q values are, to some extent, influenced by the out-of-plane diffusion as well. Both samples were measured at several temperatures between 2 and 500 K, with the temperature ramp set at 4 K/min and an additional 10 min temperature stabilization period. The sample H/MoS_2 was additionally scanned at the same temperatures after being heated to 500 K and cooled down to 2 K to check for diffusivity changes after one desorption cycle. Data were reduced within Mantid software[29] using the standard ILL reduction procedures, which include normalization to monitor, empty container subtraction, and detector efficiency correction. The reduced data do not contain any major Bragg reflections (see Figure S2 in the Supporting Information).

Numerical Simulations. Classical molecular dynamics (MD) simulations were performed using the Forcite Module of the BIOVIA Materials Studio 2020 suite (BIOVIA, Dassault Systèmes, BIOVIA Materials Studio, 20.1.0.5, San Diego). The utilized force field is pcff[30] (version 3.1), which was modified according to the paper by Liu,[31] where the force-field parameters were refined to model precisely the structural, interfacial, and mechanical properties of MoS_2 with regard to experimental data. Nondefault force field types and bonds were implemented for Mo and S depending on their position within the structure (see Figure 2). The partial charges were set to 0.5 for Mo and −0.25 for S.[31] The initial MoS_2 structure was obtained from the ICSD database with the collection code 24000, which is referenced to the work by Dickinson and Pauling.[32] The original hexagonal MoS_2 structure was redefined into an orthorhombic setup by transforming the unit cell vectors via a = (0, 1, 0), b = (1, 1, 0), and c = (0, 0, −1). Hydrogen species were simulated using the default pcff force field types h+ for protons and neutral H atoms, with a set charge of 0 for the latter, h for H_2 molecules, and hw for hydrogen in H_2O. The simulation of both H and H^+ serves the purpose of accessing the influence of charge on the diffusion characteristics of atomic hydrogen. The charge for H^+ was set to 0.9, while in the case of water, the partial charges had been assigned automatically by the force field, approximately 0.4 for hydrogen and −0.8 for oxygen. Additionally, the H_2O molecule underwent a geometry optimization procedure. The simulations of hydrogen dynamics were performed in the NVT ensemble using the Nosé−Hoover−Langevin[33,34] (NHL) thermostat and random initial velocities. The temperatures were fixed at 3, 100, 200, 300, 400, and 500 K. The total timeframe was set to 500 ps with a 1 fs time step.

For a simulation of hydrogen diffusion on a surface, a 7 × 4 supercell consisting of seven MoS_2 layers was constructed, which was merged with a 30 Å height vacuum slab, resulting in 1212 atoms in total. The four topmost layers were relaxed, and the others were set fixed. Further, five hydrogen atoms, five ions, or three H_2O or H_2 molecules, separately, were randomly placed near the surface, and the final system was subjected to geometry optimization with a fixed cell volume.

For hydrogen inside MoS_2, a 7 × 4 × 2 supercell was used, with hydrogen species placed in the middle interspace of the four-layer structure. Here, during the geometry optimization, the unit cell was optimized as well. The resulting unit cell parameters remained almost unchanged.

RESULTS AND DISCUSSION

X-ray Photoelectron Spectroscopy. The surface chemistry of the hydrogen-containing MoS_2 samples was characterized using XPS from room temperature up to 550 K. XPS allows us to identify changes of the surface chemistry due to the chemisorbed hydrogen and to test its influence on the surface oxidation state during hydrogen desorption. Pronounced chemical changes were expected for the atom beam-loaded sample, H/MoS_2, while the sample that was soaked in water, H_2O/MoS_2, was anticipated to deviate only slightly from a clean MoS_2 sample since water is not expected to bind chemically to the MoS_2 surface.

H_2O/MoS_2. As expected, the XPS spectra of H_2O/MoS_2 at room temperature exhibit an almost clean surface evidenced by

https://doi.org/10.1021/acs.jpcc.2c03848
J. Phys. Chem. C 2022, 126, 21667−21680

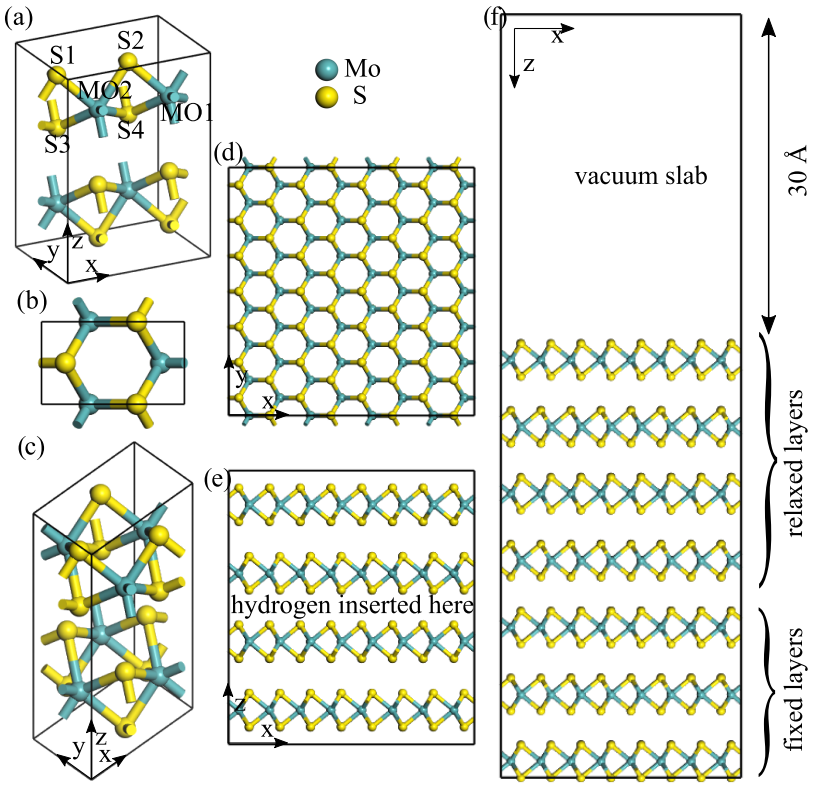

Figure 2. (a) Configuration of MoS_2 for the validation of the force fields. The labels are the force field types assigned to each atom. (b) Top view of (c) orthorhombic configuration of MoS_2. (d) Top view of the configurations that were used to simulate diffusion of hydrogen. (e, f) Side views of the configurations for the bulk and surface MoS_2 simulations, respectively.

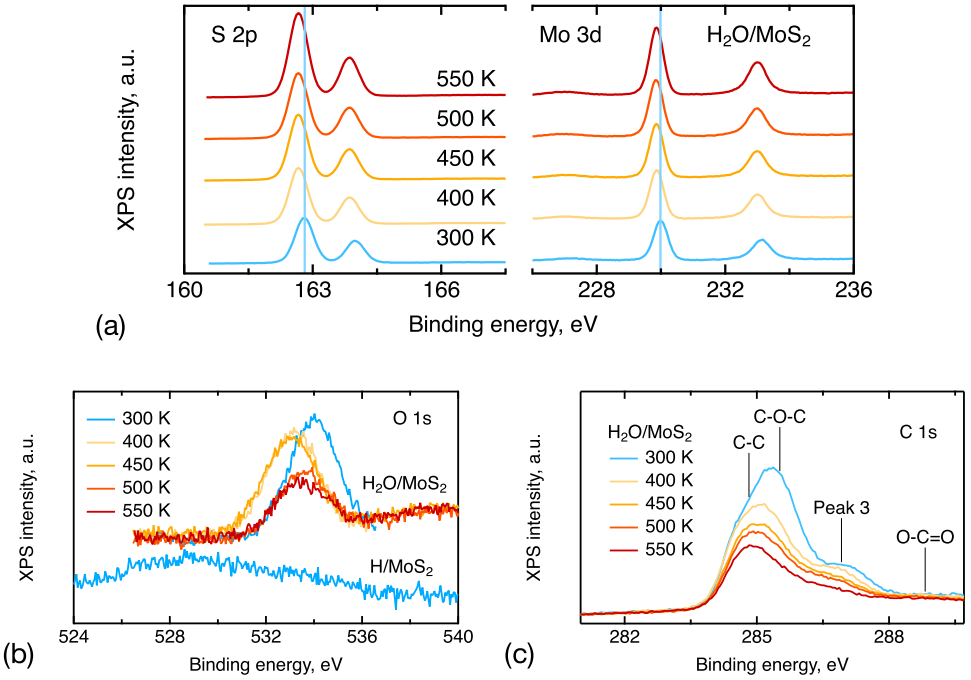

Figure 3. X-ray photoelectron spectroscopy scans of the water-loaded sample H_2O/MoS_2. (a) The S 2p and Mo 3d elemental lines were acquired at several temperatures from 300 to 550 K, indicated by different colors. For visual clarity, a vertical offset is applied to each spectrum. A blue upright line shows the position of the corresponding peak at room temperature. The displayed temperatures are the ones the sample was heated to and are slightly higher than the temperatures during measurement. (b) Scans of the O 1s line for the water-loaded sample and, as a comparison, for the hydrogen beam-loaded H/MoS_2. A vertical offset is applied to the H/MoS_2 spectrum to simplify visual comparison. (c) XPS scans of the C 1s line for the water-loaded H_2O/MoS_2. The assignment of peak 3 is ambiguous and, thus, not labeled here.

https://doi.org/10.1021/acs.jpcc.2c03848
J. Phys. Chem. C 2022, 126, 21667−21680

the binding energies of S and Mo[35,36] (Figure 3a), with a slightly reduced sulfur. This means that one-point calibration of binding energies with respect to adventitious carbon, used in this study, is adequate, and the room-temperature positions of the S and Mo elemental lines of H_2O/MoS_2 can be used within this work as a reference to a clean MoS_2 surface in terms of reduction and oxidation phenomena. We should note, however, that for the purpose of the current study, i.e., the study of dynamics of hydrogen, the absolute positions of S and Mo elemental lines are of little significance. However, we are highly interested in the shifts of the mentioned lines under temperature treatment because they show the tendency of hydrogen to create or break chemical bonds with the MoS_2 surface under induced mobility.

Heating of H_2O/MoS_2 from 300 to 400 K results in small shifts toward lower binding energy for the S 2p and Mo 3d peaks, indicating a very weak reduction process. Further temperature increase does not affect the positions of the S and Mo lines. On the other hand, during the initial heating from room temperature, the oxygen and carbon lines undergo a noticeable transformation (Figure 3b,c). The oxygen peak, the assignment of which to a specific compound will be discussed later, shifts to lower binding energies and slightly drops in intensity (Figure 3b). The carbon line consists of four peaks, positioned approximately at 284.8, 285.5, 286.9, and 288.8 eV (Figure 3c), with the last one having insignificant intensity. The first peak is attributed to adventitious carbon and acts as the binding energy reference of the present study. The second one can be assigned to carbon in the C−O−C configuration within organic molecules. Such organic molecules can be adsorbed from air while mounting the sample. The third peak possesses a binding energy that can be exhibited by a number of different compounds, and therefore, its assignment is ambiguous. One of the possibilities is carbon bound to sulfur in an S═C═S configuration.[37] The last peak at 288.8 eV could be yielded by carbon in O−C═O; however, as was already mentioned, the peak's area is negligible as compared to the other peaks. When heating the specimen from 300 to 400 K, the weight of the C−O−C line reduces almost by half, meaning that a large number of carbon atoms, which are probably bound to oxygen, are desorbed. At the same time, the O 1s line does not significantly decrease in intensity between these temperatures, i.e., we observe a lack of correlation between the changes of the areas under the peaks of O 1s, A_{O1s}, and C−O−C, A_{C-O-C}, upon heating. This suggests that most oxygen atoms are not bound to carbon at room temperature if we assume a near-linear relationship between the XPS area and the number of corresponding atoms. During heating, the ratio A_{C-O-C}/A_{O1s} takes the values 1.8, 1.4, 1.2, 1.6, and 1.6 at 300, 400, 450, 500, and 550 K, respectively, meaning that below 500 K the correlation is not observed. The O 1s line could also be yielded by molybdenum oxides; however, in this case, the corresponding binding energy is expected to lie around 530 eV,[35,36] a spectral position at which no significant signal is detected in our experiment (Figure 3c). Therefore, we conclude that, at least below 500 K, the oxygen line, observed for the H_2O/MoS_2 crystal, is yielded mostly by water, adsorbed during the loading process.

Now, we continue with the interpretation of the molybdenum and sulfur chemistry through the XPS spectra for H_2O/MoS_2. The shift of the oxygen, sulfur, and molybdenum lines to lower binding energies, occurring when heating the sample from room temperature to 400 K, can be associated with the significant desorption of C−O−C-containing molecules. Further, at higher temperatures, no significant changes are observed for the S 2p and Mo 3d lines despite considerable water desorption between 450 and 500 K. Therefore, since the alterations in the O 1s peak do not affect the chemistry of the host material, it can be concluded that water should only be physisorbed within MoS_2. Physisorption may occur within grain boundaries, cracks, and other volume defects. We note that a water molecule cannot penetrate the layered structure of MoS_2, which is obvious given its large size, and additionally observed in an aging NRRA experiment (see Figure S3 in the Supporting Information), where, over time, the bulk hydrogen concentration does not rise above the background value, given by the clean, as-received crystal. Therefore, our XPS study reveals that liquid water can access specific defective regions of MoS_2, where a larger number of active sites can be anticipated, which may be important for the catalytic mechanism.

The evolution of the O 1s line profile between 450 and 500 K suggests that the signal at 450 K consists of two peaks: one at 532.3 eV, from a species that desorbs at 500 K, and the other one at 533.4 eV, which stays unaffected at elevated temperatures. The two peaks may correspond either to water intercalated into defects of different types or to oxygen bound within H_2O and within organic molecules, provided that the disappearing peak is yielded by water. The latter option would imply a loss of quasi-elastic neutron scattering signal at 500 K, which, as will be shown later, does not occur. Therefore, we conclude that there are several types of volume defects that provide an appropriate environment for water physisorption within MoS_2 crystals. In these defects, water is constrained with different binding energies, which results in nonidentical desorption temperatures, namely, around 500 K for one species, and somewhere above 550 K for the other.

H/MoS$_2$. Now, we turn our attention to the XPS data of the H atom beam-loaded sample, H/MoS_2. We begin the description with the analysis of the oxygen and carbon lines. The O 1s peak is extremely broad and feeble (Figure 3b). It consists of several peaks; however, numerically it is not feasible to distinguish them due to weak signal. The oxygen line reaches its maximum at 529 eV, the energy region where oxygen in molybdenum oxides is expected to reside,[35,36] and then has its tail spreading until 536 eV, thus covering also the region where physisorbed water is usually observed. The peak area in the latter region is, however, much smaller than the one observed for H_2O/MoS_2, and therefore, the presence of water may be neglected. The carbon line does not show any extraordinary behavior, and thus, it was used only as a binding energy reference.

Before continuing, we would like to recall in brief the temperature treatment procedure. Each time after the specimen had been heated to an indicated temperature, the heater was turned off in order for the chamber pressure to descend to a value that allowed turning on the XPS spectrometer. During the resting time, which generally lasted around 30 min, the sample cooled down by several tens of degrees. The indicated temperature, thus, shows the temperature the crystal was heated to, which is higher than the one during measurement. This process, however, is not expected to affect the surface chemistry significantly, and therefore, the data is presumed to represent the surface state, achieved at an elevated temperature and frozen afterward. In the following, we proceed with the description of the XPS data for sulfur and

https://doi.org/10.1021/acs.jpcc.2c03848
J. Phys. Chem. C 2022, 126, 21667−21680

molybdenum. At room temperature, the S 2p and Mo 3d lines are shifted slightly to higher binding energies, corresponding to an oxidized surface. Upon heating, the surface gets reduced at 360 K (Figure 4). The reduction is accompanied by a splitting

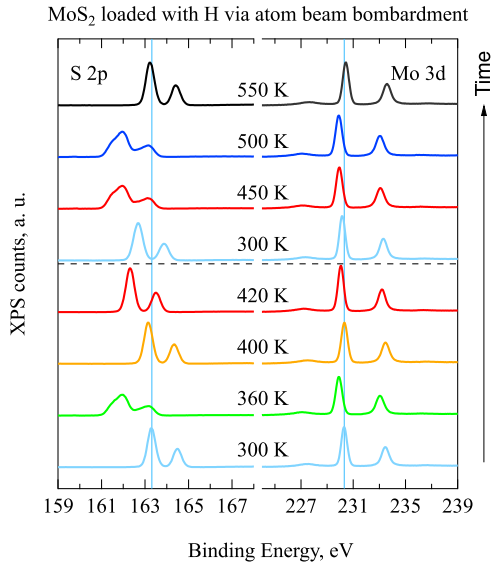

Figure 4. X-ray photoelectron spectroscopy scans of the S 2p and Mo 3d elemental lines of the atom beam-loaded sample H/MoS_2. The data were acquired at several temperatures from 300 to 550 K, which are indicated by different colors. For visual clarity, vertical offset is applied to each spectrum. A blue upright line shows the position of the corresponding peak at room temperature. The "Time" axis represents the sequential order in which the measurements were performed.

of the S 2p peak. Upon heating further to 400 K, both the sulfur and molybdenum lines reach the clean MoS_2 state. Next, at 420 K, the reduction phenomenon occurs again, but this time without a detectable splitting. Here, we note that at this temperature a strong desorption peak was encountered, leading to a much longer pressure recovery time. During the corresponding long waiting period, the sample cooled down to room temperature. The subsequent series of XPS measurements was carried out after 14 h, and the initial scan was conducted at 300 K to review the surface chemistry variations over a longer period. The S 2p line appears to shift approximately halfway toward a clean state and does not reach it. This supports our assumption that over a short time period the changes in surface chemistry are minor. When heating further to 450 and 500 K, the sample exhibits a similar pattern as observed at 360 K, with an almost identical shift and peak splitting. Then, at 550 K, the surface returns to a clean state with slightly oxidized molybdenum.

Given the observation that the water-loaded sample does not exhibit a similar behavior in terms of S 2p line shift and splitting, we conclude that the effects observed for H/MoS_2 are caused by the incorporated hydrogen. The reduction phenomenon, thus, should be attributed to hydrogen atoms, creating chemical bonds with the MoS_2 surface. This requires a source of hydrogen atoms to be present somewhere in the subsurface region. One of the possible options is hydrogen atoms incorporated into the bulk during the loading process, which migrate to the surface at elevated temperatures. The other possible source is H_2 molecules, which would be generated via recombination, given the known activity of MoS_2 in the hydrogen evolution reaction. H_2 may dissociate into H atoms on a heated MoS_2 matrix. On the other hand, considering the results of our neutron and molecular dynamics simulation studies, we will show that the samples loaded via atom beam bombardment do not contain large amounts of hydrogen molecules; therefore, their possible contribution will not be discussed explicitly. If, nevertheless, some recombined H_2 molecules are present in H/MoS_2, then their influence on the XPS spectrum will be indistinguishable from the H atoms in the −SH groups, given the similar hydrogen binding energies in these compounds.[38,39] Taking into account only the available information from XPS, the interpretation of the XPS data is not unique. In this latter sense, we will only present one of the possible scenarios in terms of different hydrogen species in the following.

Hydrogen atoms can be stored in MoS_2 combined in −SH groups, as in a perfect crystal, or in a local potential minimum near defects, such as sulfur vacancies. The binding energy of hydrogen within these species is reported to be around 0.6 eV for −SH groups and 1.3 eV for H atoms within a sulfur vacancy.[39] Experimentally, we observe the first reduction sequence at 360 K, accompanied by a peak splitting. Given the cited binding energies, this process can be assigned to the initiation of hydrogen mobility from subsurface −SH groups, which deliver new hydrogen atoms to the surface. Molybdenum sulfide layers are assembled as S−Mo−S sandwich. Therefore, it is safe to assume that, within the uppermost layer, hydrogen uptake in the outer S sublayer is different from the one in the inner S sublayer, where the former faces vacuum and the latter faces another S sublayer. This results in different reduction levels for two subsequent S sublayers and, hence, peak splitting. Further, at 400 K, all of the surface hydrogen is desorbed, resulting in a clean surface. At 420 K, hydrogen atoms constrained within sulfur vacancies start to move, providing hydrogen to the surface, thus reducing it. This reduction process becomes more pronounced at 450 K and continues up to at least 500 K, vanishing at 550 K. The fact that, in this case, total desorption requires higher temperatures or longer times suggests that the amount of hydrogen stored within sulfur vacancies is much greater than in the form of −SH groups. Here, we recall that the presented interpretation is only tentative. More experimental and calculated data are required to make a firm statement.

Neutron Time-of-Flight Spectroscopy: Hydrogen Dynamics. We now turn to the presentation of the results of the quasi-elastic neutron scattering (QENS) experiments. In QENS, the measured entity is the mobility of the sample atoms through scattering of a monochromatic beam of neutrons. Upon scattering, the mobile sample atoms exchange kinetic energy with the neutrons, which leads to a broadening of the energy distribution around the elastic scattering peak. In our experiments, the large majority of this quasi-elastic signal will stem from hydrogen because hydrogen has a substantially bigger neutron scattering cross section than all other atoms and we do not expect any significant diffusion from molybdenum or sulfur, the substrate atoms.

H_2O/MoS_2. As before, we commence our analysis with the water-loaded H_2O/MoS_2 and then continue with the H atom beam-loaded H/MoS_2. Taking a first look at the data (Figure 5a), one can observe that the quasi-elastic signal for H_2O/MoS_2 appears already at 200 K, meaning that at this temperature hydrogen atoms start moving fast enough to enter the spectroscopic window of the instrument. At 300 K,

https://doi.org/10.1021/acs.jpcc.2c03848
J. Phys. Chem. C 2022, 126, 21667−21680

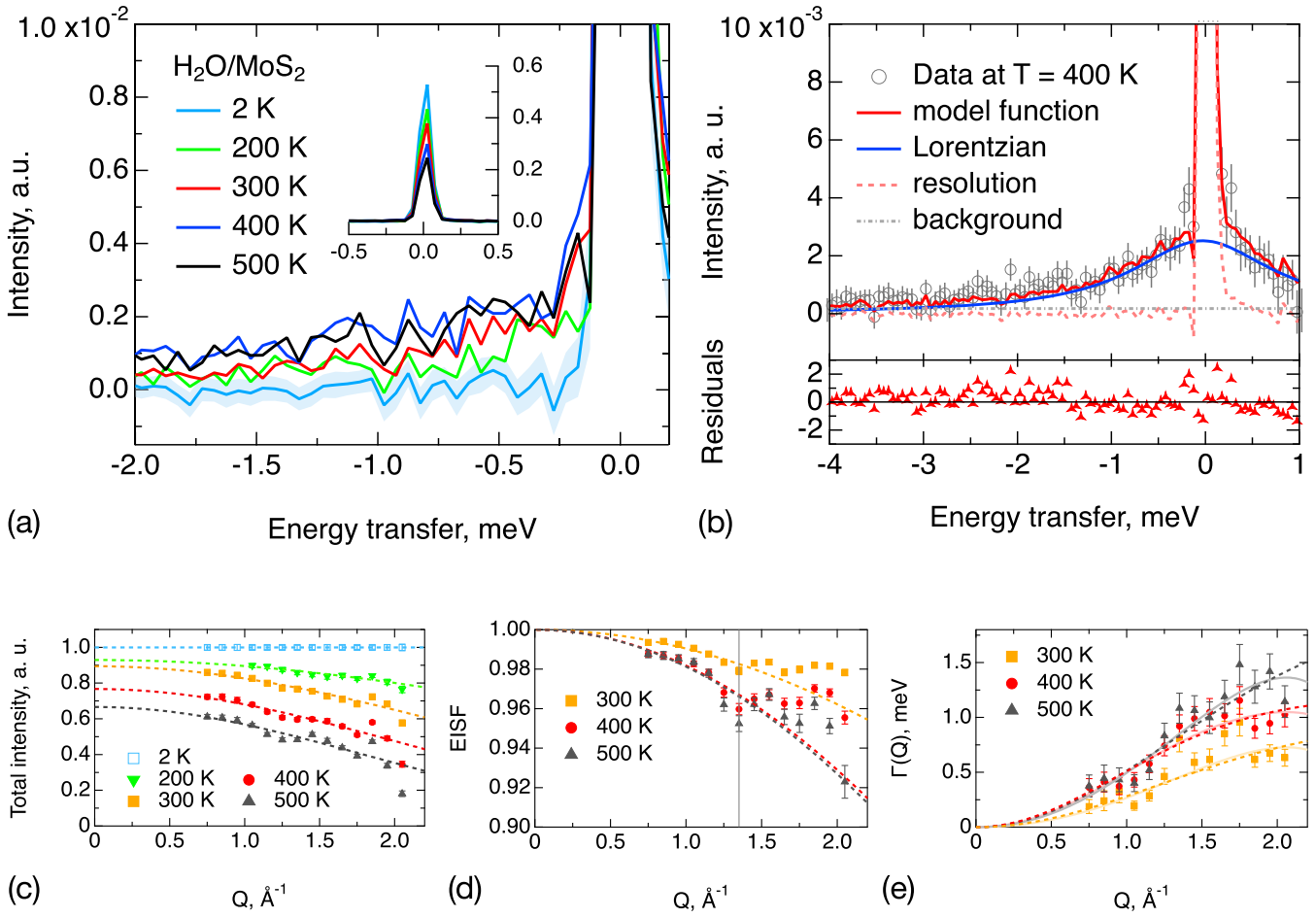

Figure 5. Overview of the QENS results for the water-loaded sample H_2O/MoS_2. (a) Quasi-elastic neutron scattering spectra of hydrogen-loaded H/MoS_2, obtained at momentum transfer $Q = 1.55$ Å^{-1}, and at various temperatures, which are indicated via coloring. The plot is scaled to display the QENS broadening. For visual clarity, the error bars are omitted for each spectrum except at 2 K, for which they are expressed as shadowing. The inset displays the same spectra in full scale in the Y axis. (b) Fit of the QENS data for H_2O/MoS_2 at 400 K and $Q = 1.35$ Å^{-1}, obtained by means of eq 2. The data points are displayed as gray circles. The model function is a red line consisting of a Lorentzian (blue line), elastic line (pale-red dashed line), and background (gray dash-dotted line). The bottom graph shows the residuals between the model function and the data, weighted for statistical errors. The elastic line is not fully represented in the plot; however, the quality of the fit around $\hbar\omega = 0$ can be assessed visually via the residual function. (c) Total neutron scattering intensity (elastic plus inelastic). Data were collected at increasing temperatures from 2 to 500 K. Experimental points are modeled with the scaled Debye−Waller law (eq 3), and the fit curves are displayed as dashed lines of corresponding colors. (d) Elastic incoherent structure factor (EISF) for hydrogen in H_2O/MoS_2. The EISF was extracted at three temperature points, indicated in the legend with corresponding colors and markers. Experimental values were approximated by means of the model for confinement within a sphere (eq 5), and the fit curves are displayed as dashed lines of corresponding colors. Data points to the left of the vertical line were used for the quantitative fit, while the points to the right are significantly influenced by elastic peaks and were, hence, not used for the fits. The error bars at 300 K are smaller than the markers. (e) Width of the QENS broadening Γ, estimated at three temperature points and displayed as colored markers according to the legend. The fits by means of the Hall−Ross (HR) model are shown as dashed lines and by the Chudley−Elliott (CE) model as straight pale lines. The latter model is unstable since no data are available beyond the apex, after which bending downward occurs.

the intensity of the QENS signal increases substantially, and it stays at a similar level beyond this temperature. The data were fitted with a general model, which consists of a sum of an elastic line and one Lorentzian, describing the quasi-elastic broadening

$$S(Q, \omega) = A_{el}(Q)S_{res}(Q, \omega) + A_{qe}(Q)L(\Gamma(Q), \omega) * S_{res}(Q, \omega) + B \quad (2)$$

where $A_{el}(Q)$ and $A_{qe}(Q)$ are intensities of elastic and quasi-elastic scattering, respectively; $S_{res}(Q, \omega)$ is the instrument resolution function, i.e., the spectra obtained at 2 K where no detectable atomic motion is anticipated; $L(\Gamma(Q), \omega) = \frac{1}{\pi}\frac{\Gamma(Q)}{\omega^2 + \Gamma(Q)^2}$ is a normalized Lorentzian function with a half width at half-maximum (HWHM), $\Gamma(Q)$; B is a constant background term; and * represents a convolution action. Apparently, one Lorentzian is sufficient to describe the data of H_2O/MoS_2 (Figure 5b), and the introduction of a second Lorentzian does not significantly improve the fit results in terms of χ^2 statistics. Therefore, we may conclude that only one diffusion mode is observed for H_2O/MoS_2.

By looking at the total scattering intensity $A_{total}(Q) = A_{el}(Q) + A_{qe}(Q)$ (Figure 5c), it becomes evident that some signal is lost when heating the sample. Also, we note small peaks around 1.5 and 1.9 Å^{-1}, which could be caused by various compounds possibly existing in the system; however, the determination of an exact source is not important for the current study. For the interpretation of the total scattering

https://doi.org/10.1021/acs.jpcc.2c03848
J. Phys. Chem. C 2022, 126, 21667−21680

intensity behavior, the peaks do not play a major role, but further in the analysis of the elastic incoherent structure factor, their effect will be significant and easily observable. $A_{total}(Q)$ can be expressed as a product of a Q-independent constituent $K(T)$, which represents the amount of hydrogen in the sample and, hence, depends on temperature and the Debye−Waller factor

$$A_{total}(Q) = K \exp(-Q^2\langle u^2\rangle/3) \tag{3}$$

where $\langle u^2\rangle$ stands for the mean square displacement of H atoms. During heating, some hydrogen could desorb and leave the system, thus decreasing the $K(T)$ coefficient, which is normalized to be equal to unity at 2 K. By fitting the data to eq 3, it is possible to estimate $K(T)$, which appears to gradually decrease with rising temperature (Figure 5c), decaying from 0.93 at 200 K to 0.67 at 500 K. Thus, even at the highest scanned temperature, the amount of water in the sample remains significant. A similar situation is observed in the XPS experiment, where the oxygen line remains strong at 550 K.

Now, we proceed to the analysis of an eventual spatial confinement of water molecules. In QENS, the elastic incoherent structure factor, $A_0(Q)$, (EISF), allows us to determine if mobility is spatially constrained (Figure 5d). The EISF provides information about the shape and size of a space region accessible to a hydrogen atom and can be evaluated as a ratio of elastic intensity to total intensity[40]

$$A_0(Q) = \frac{A_{el}(Q)}{A_{el}(Q) + A_{qe}(Q)} \tag{4}$$

Unfortunately, due to the already mentioned elastic peaks, the data beyond Q = 1.4 Å^{-1} are unsuitable for the analysis of EISF. Nevertheless, an attempt was made to fit the whole range, which did not lead to qualitatively different results, which would affect the interpretation that is given below. Therefore, this analysis is brought to the Section S1, and further in the text, we will only refer to the analysis for the Q range below 1.4 Å^{-1} since it is more justified. The Q region up to 1.4 Å^{-1} allows one only to estimate the size of the confining volume but provides no conclusive information on its shape. Therefore, for a quantitative analysis, a basic model of a confinement within an impermeable sphere of a radius R_c was used[41]

$$A_0(Q) = A_0(0)\cdot\left(\frac{3j_1(QR_c)}{QR_c}\right)^2 \tag{5}$$

where $j_1(QR_c)$ is a spherical Bessel function of the first kind and first order and the factor $A_0(0)$ accounts for the fraction of hydrogen that is constrained. The chosen model describes the data well, but the fits of the data yield an unexpectedly small radius of confinement, R_c = 0.30 ± 0.01 Å, at elevated temperatures and an even smaller radius, R_c = 0.20 ± 0.01 Å, at 300 K. These values could be influenced by the presence of immobile hydrogen within the sample. Here, we use the notion "immobile" to refer to hydrogen atoms that are moving too slowly to yield a QENS broadening within the resolution window of the spectrometer. The XPS experiment revealed that water is constrained within different local MoS_2 environments, having variable binding energies there. This suggests that the diffusion rate of H atoms may also vary from one local environment to another. Very slow hydrogen, thus, contributes to the elastic line, increasing the EISF and decreasing the observed apparent confining radius. Nevertheless, the R_c remains much smaller than the gyration radius of H in a water molecule. This means that the detected motion should not be attributed to a full revolution of hydrogen around an oxygen atom. To acquire a better insight into which kind of hydrogen diffusion is observed, the analysis of the Lorentzian line width is required.

Apart from a full revolution, hydrogen atoms may also perform rotational motion around, for instance, an axis that is parallel to the line connecting two H atoms in H_2O and that passes through the O atom. In this case, the Lorentzian width, $\Gamma(Q)$, should be constant over the scanned momentum transfer region. However, the experimental values clearly show the presence of translational diffusion with a jumplike behavior, which is indicated by a rise of $\Gamma(Q)$ at low Q, and its saturation above 1.7 Å^{-1} (Figure 5e). Jump diffusion in a liquid is usually treated in terms of the Singwi−Sjölander (SS) model,[42] which assumes an exponentially decaying distribution of jump lengths

$$\rho(r) = r/r_0^2 \exp(-r/r_0) \tag{6}$$

Along with the SS model, we have also tested the Hall−Ross[43] (HR) and Chudley−Elliott[44] (CE) models on our set of data. The former utilizes a normal distribution of jump distances

$$\rho(r) = \frac{2r^2}{r_0^3\sqrt{2\pi}} \exp(-r^2/2r_0^2) \tag{7}$$

and the latter assumes diffusion over a discrete array of jump sites of a Bravais lattice. The explicit formulae for the Lorentzian widths in these models are

$$\Gamma_{SS}(Q) = \frac{\hbar D_{SS}Q^2}{1 + \tau_{SS}D_{SS}Q^2}$$

$$\Gamma_{HR}(Q) = \frac{\hbar}{\tau_{HR}}\cdot[1-e^{-\tau_{HR}D_{HR}Q^2}]$$

$$\Gamma_{CE}(Q) = \frac{3\hbar}{4\tau_{CE}}[1-J_0(Q_{\|}l)] \tag{8}$$

where D is the diffusion coefficient, τ is the residence time between jumps, l is the distance between jump sites, $\hbar$ is the reduced Planck's constant, and $J_0(Q_{\|}l)$ is the Bessel function of the first kind and order zero with $Q_{\|} = Q\sin(\phi + \arcsin(Q\lambda/4\pi))$ being the projection of the $\mathbf{Q}$ vector on the MoS_2 basal plane. Here, we used a representation of the CE model developed for a two-dimensional (2D) hexagonal array of jump sites,[16] which satisfies the structure of MoS_2. However, given the statistical errors of the data, the exact pattern of the jump site distribution is not significant. All three models produce a satisfactory description of the data. Unfortunately, the fits of the CE model became unstable and yielded large errors in the fit parameters due to a lack of data points beyond 2 Å^{-1}, which are important to access the sine-like features of the CE model. Therefore, only the SS and HR models will be discussed further. Their results are summarized in Table 1. The diffusion coefficient increases when the sample is heated from room temperature to 400 K. At 500 K, it does not increase further within the experimental error bars.

Given the above results, we propose two possible scenarios for the translational diffusion of hydrogen in H_2O/MoS_2. As already noted, water molecules should be adsorbed in small voids or cracks in the material. The first option is diffusion of H_2O molecules as a whole around a defect domain, which

https://doi.org/10.1021/acs.jpcc.2c03848
J. Phys. Chem. C 2022, 126, 21667−21680

Table 1. Results of the Analysis of QENS Broadening for H_2O/MoS_2 by means of the Singwi–Sjölander and Hall–Ross Models[a]

T, K	$\sqrt{\langle l^2 \rangle}$, Å	τ_{res}, ps	D, 10^{-8} m^2/s
Singwi–Sjölander			
300	1.1 ± 0.2	0.4 ± 0.1	0.5 ± 0.1
400	1.6 ± 0.2	0.4 ± 0.1	1.1 ± 0.2
500	1.1 ± 0.2	0.2 ± 0.1	0.9 ± 0.1
Hall–Ross			
300	1.4 ± 0.2	0.7 ± 0.1	0.5 ± 0.1
400	1.8 ± 0.2	0.6 ± 0.1	1.1 ± 0.2
500	1.4 ± 0.2	0.3 ± 0.1	0.9 ± 0.1

[a]The average jump distance is $d = \sqrt{\langle l^2 \rangle}$, the residence time between jumps is τ_{res}, and the diffusion coefficient is D.

provides a small enough binding energy of water molecules inside of it. Provided the domain hosts several H_2O molecules, they may collide with each other performing a motion, which is generally described via liquid diffusion models, such as SS and HR. The other option is a clustering of water molecules and subsequent hopping of hydrogen atoms from one oxygen to another or to sulfur and back.

H/MoS$_2$. Now, we turn to the H atom beam-loaded H/MoS_2. Here, the 200 K spectra showed no observable quasi-elastic broadening, and hence, they were used as resolution functions. During the initial heating run, the quasi-elastic signal rose significantly at 300 K and continued increasing up to 400 K (Figure 6a). Further, at 500 K, the QENS signal vanished, returning to the spectrum observed at 200 K. This indicates a loss of almost all of the hydrogen that was mobile at 400 K. Since the sample holder was open to the cryofurnace environment, the desorbed hydrogen was not expected to be readsorbed when cooling down. This is exactly what was observed during the second heating run: the absence of any significant QENS signal. Therefore, the second run was used as a measure of the host scattering, which includes immobile hydrogen species and a small contribution from MoS_2. The second heating run spectra, thus, were subtracted from the corresponding first heating run data to minimize the influence of the scatterers not under study.

To describe the corrected data, eq 2 was used, with $S_{res}(Q,\omega)$ being the corresponding 200 K spectrum. The QENS signal at both 300 and 400 K is rather scarce. Therefore, only the high Q data could be exploited for a quantitative analysis. Clearly, one Lorentzian model is sufficient to fit the profile of the experimental spectra (Figure 6b), and no additional peak is required. This is different from what was

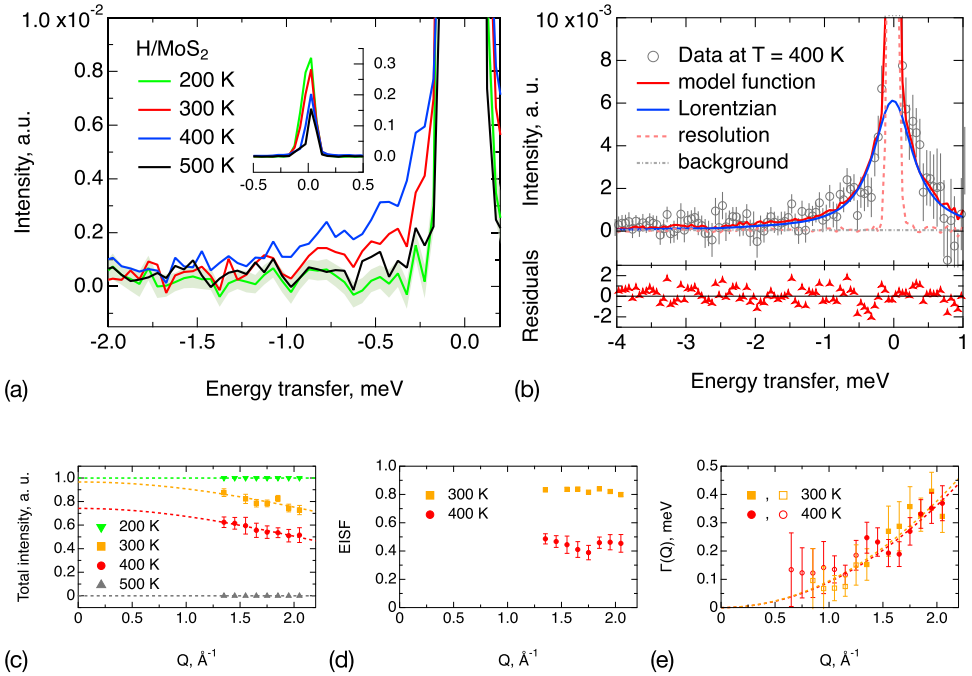

Figure 6. Overview of the QENS results for the sample H/MoS_2 that was loaded by atom beam bombardment. (a) Quasi-elastic neutron scattering spectra of hydrogen-loaded H/MoS_2, obtained at momentum transfer Q = 1.85 Å^{-1} and at various temperatures, which are indicated via coloring. The plot is scaled to display the QENS broadening. For visual clarity, the error bars are omitted for each spectrum except at 200 K, for which they are expressed as shadowing. The inset displays the same spectra in full scale in the Y axis. (b) Fit of the QENS data for H/MoS_2 at 400 K and Q = 1.85 Å^{-1}, obtained by means of eq 2. The data points are displayed as gray circles. The model function is a red line consisting of a Lorentzian (blue line), elastic line (pale-red dashed line), and background (gray dash-dotted line). The bottom graph shows the residuals between the model function and the data, weighted for statistical errors. The elastic line is not fully represented in the plot; however, the quality of the fit around $\hbar\omega$ = 0 can be assessed visually via the residual function. (c) Total neutron scattering intensity (elastic plus inelastic). Data were collected at increasing temperatures from 200 to 500 K. Experimental points are modeled with the scaled Debye–Waller law (eq 3), and the fit curves are displayed as dashed lines of corresponding colors. (d) Elastic incoherent structure factor (EISF). The EISF was extracted at two temperature points from the first heating run, indicated in the legend with corresponding colors and markers. The error bars at 300 K are smaller than the markers. (e) Width of the QENS broadening Γ, extracted at two temperature points and displayed as colored markers according to the legend. The full markers indicate that the points were obtained via the default model given by eq 2, while for the points with hollow markers, the intensity of the Lorentzian was fixed. The fits by means of the DQ^2 model for Brownian diffusion are shown as dashed lines.

https://doi.org/10.1021/acs.jpcc.2c03848
J. Phys. Chem. C 2022, 126, 21667–21680

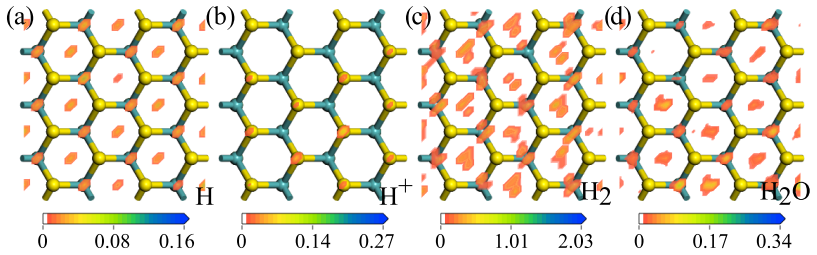

Figure 7. Top views of the results from adsorption dynamics calculations, which show preferred sites for hydrogen. The color shows the density of hydrogen on the surface. The inhomogeneity of the hydrogen density is caused by the limited sampling statistics of the adsorption calculations.

observed previously for the MoS_2 crystals that were electrolytically loaded with hydrogen,[16] where two diffusion modes were detected. The total scattering intensity, $A_{total}(Q)$, was fitted to the already mentioned scaled Debye–Waller law (eq 3). The extrapolation of $A_{total}(Q)$ to $Q = 0$ Å^{-1} reveals that at room temperature the overall amount of hydrogen is almost the same as at 200 K (Figure 6c). The desorption starts when heating the sample to 400 K, which leads to a drop in the amount of hydrogen by 26%. Further heating to 500 K results in total loss of mobile hydrogen. In the XPS experiment, we observed hydrogen desorption at a somewhat higher temperature, 550 K. This difference is caused by a shorter period between the scans in XPS than in the neutron measurement, i.e., in the X-ray experiment, hydrogen did not have enough time to fully desorb below 550 K.

Next, we examine the effect of hydrogen confinement in H/MoS_2. We recall that the data were collected for the in-plane geometry, which means that the diffusion parallel to the MoS_2 basal planes is studied. The EISF appears to be constant within the error bars at both 300 and 400 K, meaning that no spatial restrictions for hydrogen diffusion are observed (Figure 6d). However, the value of the extrapolation to $Q = 0$ Å^{-1} changes under temperature treatment, decaying from 0.83 at 300 K to 0.45 at 400 K. This value represents the ratio of immobile hydrogen to the total amount of hydrogen in the sample. It is evident that at 300 K only a small fraction of H atoms perform movement fast enough to be detected in the experiment. Further, at 400 K, more hydrogen centers get activated and around a half of the H atoms become mobile. The total hydrogen mobilization is anticipated somewhere between 400 and 500 K, since at the latter temperature, any QENS signal is lost. We note, taking into account the reduction procedure, that this does not forbid the presence of any hydrogen species, which remain immobile even at 500 K. From NRRA, it is deduced that some amount of immobile hydrogen is present up to 700 K.

For the estimation of Lorentzian widths, to obtain more data points, an alternative fitting approach was used. Data at high Q were fitted as described previously in the text, while spectra at low Q were fitted with the same equation but with the Lorentzian area fixed. Since in this range all of the intensity parameters vary only slightly, the approximation must yield the quasi-elastic broadening close to the correct one. Nevertheless, in Figure 6e, the two ranges are depicted explicitly to stress the different fitting procedures. The width of the QENS broadening, $\Gamma(Q)$, increases with Q and does not reach a plateau within the available Q region, which is a common feature for a continuous Brownian diffusion[26] (Figure 6e). Such behavior, of course, can also be described by means of jump-diffusion models with a continuous distribution of jump lengths, like the Singwi–Sjölander (SS) model. However, this leads to overparametrization, and therefore, in this case, jump-diffusion models become less trustworthy. On that accord, we will continue the interpretation in terms of Brownian motion. Interestingly, the diffusion coefficient, D, at 300 and 400 K is mostly the same, amounting to 1×10^{-9} m^2/s. Unfortunately, with only two temperature points available for analysis, we cannot present an unambiguous interpretation of the diffusion pattern of H atoms in MoS_2. Atomic hydrogen motion seems to be slower in MoS_2 than on the surface of Pt,[45] and the diffusion coefficient of the former does not vary significantly between room temperature and 400 K.

Molecular Dynamics Simulations. Recently, Liu et al.[31] have reported simulation parameters for MoS_2, which can be used with various force fields to accurately simulate structural and interfacial properties. In particular, the simulation of wetting MoS_2 with water yielded contact angles in good agreement with the experiment.[31] Here, we tried to use these parameters with several force fields (cvff, Dreiding and pcff) to qualitatively study the dynamics of hydrogen in MoS_2, which we observed in our experiments. The results may help better understand which motion modes of various hydrogen species in MoS_2 can be described classically and which are strongly affected by the creation and breaking of covalent bonds, the phenomenon neglected in the classical MD simulations used here.

The molecular dynamics simulations were performed for two configurations of hydrogen: on the surface of MoS_2 and in its bulk. We simulated four hydrogen species, namely, neutral H atoms, positively charged H^+ ions, H_2 molecules, and water molecules. The comparison of the simulations of H and H^+ allows us to assess the influence of hydrogen charge on its diffusion pattern, which is important in view of a possible electron exchange with the MoS_2 matrix. The examination of H_2 diffusion, which was not experimentally assessed in the current study, was carried out to ensure that the observed motion in H/MoS_2 was not due to recombined H_2. Among the sampled force fields, only pcff allowed hydrogen to move across the bulk of MoS_2 and, hence, this force field was used for further studies.

We begin the description with the results for hydrogen diffusion on the surface of MoS_2 (see Figures 7 and S5). When neutral hydrogen atoms are placed on the surface, they desorb already at the lowest simulated temperature of 3 K. Hence, no surface diffusion could be observed. H^+ ions, on the contrary, are attracted to S atoms via Coulomb forces and stay on the surface until the temperature rises to 200 K. Between 100 and 200 K, hydrogen ions occasionally hop from one sulfur atom to another, with a frequency that increases with temperature. This type of diffusion would probably be difficult to observe experimentally since at low temperatures the diffusion is very slow and the increase in temperature is directly connected to

https://doi.org/10.1021/acs.jpcc.2c03848
J. Phys. Chem. C 2022, 126, 21667–21680

the strength of H desorption. H_2, similar to neutral atoms, is barely attracted to the MoS_2 surface and leaves it at 100 K. Water molecules, on the contrary, position themselves on top of Mo atoms and stay on the surface almost up to 500 K. The desorption temperature can be increased even higher by creating a sulfur vacancy and placing a H_2O molecule in its vicinity. This behavior is in line with our XPS study, where we observed a significant drop in the oxygen signal between 450 and 500 K, as well as with the QENS results, where a substantial amount of hydrogen was still present at 500 K. The simulated desorption temperature of neutral H atoms is too far from our experimental observations; hence, the creation of chemical bonds must play a role in H adsorption and should not be neglected in this kind of calculation. The desorption temperature of hydrogen ions is closer to the experimental values, but it is still underestimated.

The possibility of penetrating the layers of MoS_2 was calculated for H, H^+, and H_2 (Figure 8). It was not calculated

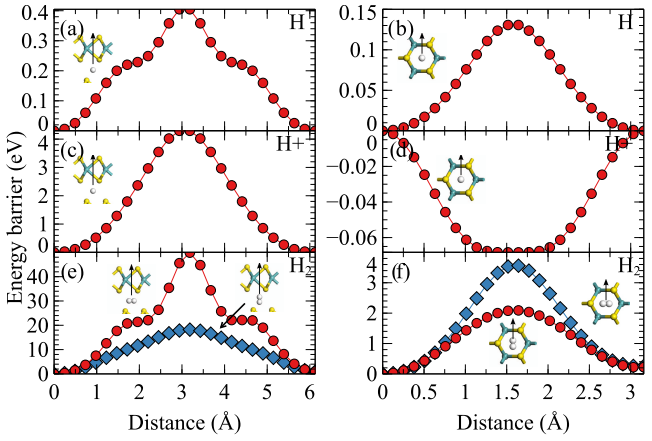

Figure 8. Diffusion barriers for H, H^+, and H_2. (a), (c), and (e) are the barriers when crossing the S−Mo−S layer through a hole. (b), (d), and (f) are the barriers when hydrogen moves parallel to the layers in the space between layers from one hexagonal site to another.

for H_2O since it is obvious that water molecules, due to their size, cannot pass through a defect-free layer. The calculation was carried out manually by placing the atom or molecule at the initial position and subsequently shifting it toward the destination and calculating its energy at several intermediate points. This method is a rough estimation of the diffusion barriers for different hydrogen species since the lowest energy path is not necessarily a straight line and is intended to be used for intracomparison rather than for a precise estimation. The calculated energy barrier appeared to be much higher for the ions than for neutral atoms, where it is approximately 4 eV for the former and 0.4 eV for the latter. Apparently, the difference is caused by the Coulomb repulsion by the Mo atoms. This information suggests that the bombardment of MoS_2 with neutral H atoms can relatively easily deliver them a few layers deep into the material. Then, after losing kinetic energy, protiums bind to sulfur and layer penetration becomes hindered. The diffusion barrier for migration parallel to the MoS_2 layers from one hexagonal site to another is at a similar level for both H and H^+, below 0.15 eV, which is significantly lower than the one for layer penetration. H_2 diffusion is hindered in both directions, with a very high 20 eV barrier for relocation from one interlayer space to another, even with the H_2 molecule aligned perpendicular to the layers (Figure 8). Jumps between hexagonal sites are also improbable and depend on the orientation of the molecule, although the barrier is much lower, 2 eV. Hence, if any recombined H_2 is present in the bulk of a MoS_2 crystal, it is not expected to leave the crystal at room temperature.

The diffusion of H and H^+ in the bulk of MoS_2 exhibits a jumplike behavior; however, the jump site geometries are different (Figures 9 and S3). Neutral atoms favor staying between six sulfur atoms of two adjacent layers, while ions are mostly located at a line connecting two nearest S atoms from adjacent layers. We will call the former the hexagonal site, and the latter, the bridge site. The hopping usually occurs as a series of two or three consecutive jumps and is heavily correlated with the shearing of MoS_2 layers (Movies S1 and S2 in the Supporting Information). The diffusion coefficient, D, was estimated on the basis of fitting the QENS spectra, calculated from the simulated hydrogen trajectories. Despite the fact that the layer penetration barrier is smaller for neutral atoms than for ions, the diffusion coefficient for the motion between layers shows the opposite behavior. For H, the obtained D rises from 3.5 to 7.5 × 10^{-8} m^2/s at 300 and 500 K, respectively, while for H^+, it first leaps up from 2.2 to 21.3 × 10^{-8} m^2/s between 300 and 400 K and then decays to 10.3 × 10^{-8} m^2/s at 500 K. This behavior is directly connected to the shearing of MoS_2 layers. A protium, being added to the matrix, does not disturb the structure significantly, and the mean square displacement of sulfur atoms remains close to its value for a clean MoS_2. A positive proton, on the other hand, destabilizes the matrix completely, inducing a large displacement of S atoms, which at 500 K results in the formation of a new stable structure, which is closest to $P\bar{6}m2$. Such instability drives hydrogen movement and causes a large diffusion coefficient for H^+ at 400 K. The decrease of D at 500 K is

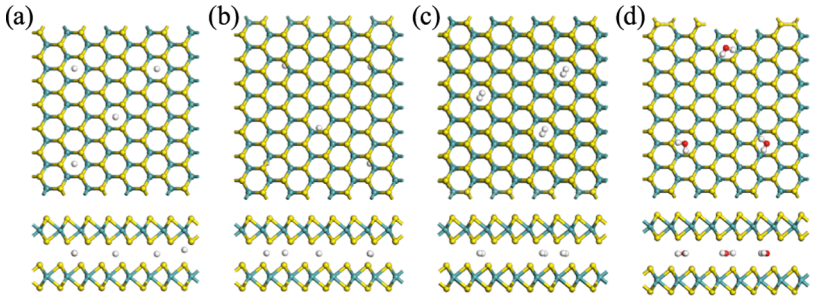

Figure 9. Hydrogen that is inside the bulk MoS_2 at 3 K. (a)−(d) show top views (top) and side views (bottom) of the model for H, H^+, H_2, and H_2O, respectively.

https://doi.org/10.1021/acs.jpcc.2c03848
J. Phys. Chem. C 2022, 126, 21667−21680

the result of a more stable structure. We note that in a real crystal a disorder of this kind is less likely to occur since a substantial amount of hydrogen is only present up to ∼100 nm below the surface; beyond this depth, there is stable, hydrogen-free molybdenum sulfide. The calculated diffusion coefficients are 1−2 orders of magnitude higher than observed in the experiment, meaning that phenomena neglected by our simulation, for instance, the creation and breaking of covalent bonds, play an important role in the rate of H/H^+ diffusion in MoS_2. Nevertheless, our simulations propose that the structural instability of the host matrix caused by the presence of H^+ heavily impacts the diffusion rate of hydrogen. This could explain the weak temperature dependence of the experimentally observed diffusion coefficient.

Water molecules in the bulk of MoS_2 stay in hexagonal interlayer sites with the oxygen atom pinned in the center and almost immobile (Figure 9). The water hydrogen atoms perform rotational motion around the oxygen (Movies S3 and S4 in the Supporting Information). The main mode is 2D rotations in plane, parallel to MoS_2 layers (c rotational axis). As the temperature rises, out-of-plane swings intensify and occasionally full revolutions around the rotational axis happen. The simulated QENS broadening is constant versus Q and amounts to 4 meV already at 100 K, rising with temperature. Therefore, it is not surprising that in the experiment, no rotational motion is detected since it would result in a Lorentzian broadening that is large enough to be interpreted as a constant background, i.e., it is too fast for the spectroscopic window of our neutron spectroscopy experiments. The translational diffusion observed in the TOF study, thus, cannot be yielded by water molecules constrained in a perfect crystal and must be caused by structural defects, the exact configuration of which is still under question.

In a similar manner, H_2 molecules are trapped in the centers of hexagonal interlayer sites. However, their motion is restricted from performing a full revolution around the molecule's center of mass (Movies S5 and S6 in the Supporting Information). Instead, the molecule undergoes random jumplike reorientations mostly parallel to the MoS_2 layers. The displayed quasi-elastic broadening is constant versus Q and increases from 0.2 to 2 meV from 100 to 500 K, respectively. These values lie well within the spectroscopic window of the exploited neutron spectrometer; therefore, such diffusion must be observable in our experiment. However, the experimental results clearly show only one diffusion mode, the QENS broadening of which follows the DQ^2 law. Moreover, at 500 K, any QENS signal is lost, while the simulations suggest that H_2 cannot yet leave the crystal at this temperature. Following the same interpretation as for H_2O, hydrogen molecules may also be trapped in large voids or grain boundaries inside the crystal; however, even in this case, they must desorb either at low (surface) or at very high (bulk) temperatures. Therefore, we can conclude that in the current study of H/MoS_2 we have not experimentally observed any signs of recombined H_2 diffusion. This also suggests that H_2 dissociation cannot be a source of H atoms, which contribute to the reduction process detected in the XPS experiment.

CONCLUSIONS

In summary, the adsorption behavior and motion of water and atomic hydrogen in MoS_2 have been studied.

Exposed to liquid water, MoS_2 crystals tend to absorb a substantial amount of H_2O molecules, which are partially restrained within the host matrix up to the highest temperatures of our experiments, 500 K. The synoptical consideration of all methods points to physisorption in voids or cracks of the material, and we find that there is no intercalation between perfect MoS_2 bilayers. The possibility of a mobile electrolyte accessing the inner surfaces of the crystalline material may be important for the electrocatalytic performance of MoS_2. The motion of H_2O molecules is similar to diffusion in liquid water: it is dominated either by movement of intact molecules in the volume of the void or by hopping of protons between oxygen and sulfur, similar to proton conduction in bulk water.

X-ray photoelectron spectroscopy reveals that under temperature treatment the surface of the H atom-loaded MoS_2 crystal undergoes a series of reduction−oxidation cycles. This effect is due to hydrogen migration and is mainly observed for sulfur atoms. The reduction is attributed to the formation of S−H groups by attachment of hydrogen to the surface. Surface reduction is followed by reoxidation under hydrogen desorption, as expected for recombinative desorption of H_2. Within the studied range of temperatures, two reduction−oxidation cycles were observed. The first one was between 360 and 400 K, which was assigned, based on the bond strength, to the mobilization of hydrogen within subsurface S−H groups, along with dissociation of the possibly generated H_2 molecules. The second cycle occurring between 420 and 550 K was assigned to hydrogen atoms bound within S vacancies or other defective sites, which provide a similar hydrogen binding energy. During the first cycle, these atoms did not have enough energy to leave their traps and were, in terms of the time scale of our study, immobile. The number of H atoms activated during the second cycle was found to be greater than the one for the first cycle, as indicated by the temperature range span of the reduction process.

As far as hydrogen diffusion is concerned, we find that in the present study for H/MoS_2 the mobile species is clearly $H^{0/+}$, i.e., H in the form of atoms or protons, as evidenced by our QENS and MD simulations results. The QENS data exhibit only one motion mode in contrast to our previous study on electrolysis-loaded samples,[16] where we found clear evidence of two diffusion processes. For the electrolytically loaded samples, the motion of hydrogen molecules within the material was identified as the major contribution leading to the fast diffusion process. Since H_2 does not diffuse through MoS_2 layers, these molecules must have been formed by recombination of H atoms within the material. This process, apparently, does not dominate in the case of H atom beam loading. Nevertheless, the slower diffusion component of the electrolytically loaded samples displays a similar broadening as the motion observed in the present experiments and could indeed be caused by $H^{0/+}$ diffusion.

The study of the in-plane movement of atomic hydrogen, i.e., motion parallel to the MoS_2 layers, discovered a moderately swift diffusion with $D \approx 1 \times 10^{-9}$ m^2/s. The data suggests the interpretation in terms of Brownian diffusion; however, within the explored momentum transfer range, Brownian and jump diffusion with a continuous distribution of jump lengths could not be resolved with confidence. No spatial confinement was observed at the examined temperatures, as expected for diffusing species of the size of a H atom (or proton). The diffusion coefficient appeared to be the same at 300 and 400 K; however, two data points are not enough to establish a statistically justified interpretation. Compared to atomic hydrogen diffusion on a Pt surface,[45] the experimentally

https://doi.org/10.1021/acs.jpcc.2c03848
J. Phys. Chem. C 2022, 126, 21667−21680

observed motion of H atoms in crystalline MoS_2 is slower by an order of magnitude, but, as numerical simulations suggest, it could be largely influenced by the particular structure of MoS_2, which is known to have two naturally occurring polytypes, namely, 2H-MoS_2 and 1T-MoS_2. Therefore, the diffusion of hydrogen still seems to be able to play a role in the catalytic mechanism since it provides a means to vacate an active site by making available nonreactive parts of the surface.

■ ASSOCIATED CONTENT

Supporting Information

The Supporting Information is available free of charge at https://pubs.acs.org/doi/10.1021/acs.jpcc.2c03848.

Additional details on sample preparation as well as additional data from measurements and computational simulations (PDF)

Movies of the molecular dynamics simulations (ZIP)

■ AUTHOR INFORMATION

Corresponding Author

Peter Fouquet − *Institut Laue-Langevin, 38042 Grenoble, France;* orcid.org/0000-0002-5542-0059; Email: fouquet@ill.fr

Authors

Vitalii Kuznetsov − *Institut Laue-Langevin, 38042 Grenoble, France; Westfälische Hochschule, Gelsenkirchen, Bocholt, Recklinghausen, 45665 Recklinghausen, Germany*

Leran Lu − *Institut Laue-Langevin, 38042 Grenoble, France; Université de Lyon, 69361 Lyon, France*

Michael M. Koza − *Institut Laue-Langevin, 38042 Grenoble, France*

Detlef Rogalla − *RUBION, Ruhr-Universität Bochum, 44801 Bochum, Germany*

Varvara Foteinou − *RUBION, Ruhr-Universität Bochum, 44801 Bochum, Germany*

Hans-Werner Becker − *RUBION, Ruhr-Universität Bochum, 44801 Bochum, Germany*

Alexei Nefedov − *Institut für Funktionelle Grenzflächen (IFG), Karlsruher Institut für Technologie (KIT), 76344 Eggenstein-Leopoldshafen, Germany;* orcid.org/0000-0003-2771-6386

Franziska Traeger − *Westfälische Hochschule, Gelsenkirchen, Bocholt, Recklinghausen, 45665 Recklinghausen, Germany*

Complete contact information is available at: https://pubs.acs.org/10.1021/acs.jpcc.2c03848

Notes

The authors declare no competing financial interest.

■ ACKNOWLEDGMENTS

This work was financed within the scope of the joint Ph.D. project ref ILL-1709.1 between Institut Laue-Langevin (ILL) and Westfälische Hochschule. The paper is based on experiments performed at the IN6-SHARP instrument at Institut Laue-Langevin, Grenoble, France. The project has received support from the European Union's Horizon 2020 research and innovation program under grant agreement no. 730872 CALYPSO plus for the work at the HZB BESSY II synchrotron, Berlin, Germany. The authors want to thank HZB for the allocation of synchrotron radiation beam time at BESSY II via project 192-08548 CR. The authors want to thank ILL for the allocation of neutron beam time.

■ REFERENCES

(1) Carmo, M.; Fritz, D. L.; Mergel, J.; Stolten, D. A comprehensive review on PEM water electrolysis. *Int. J. Hydrogen Energy* **2013**, *38*, 4901−4934.

(2) Chisholm, G.; Cronin, L.*Storing Energy*; Elsevier, 2016; pp 315−343.

(3) Marcinkoski, J.; Spendelow, J.; Wilson, A.; Papageorgopoulos, D.*DOE Hydrogen and Fuel Cells Program Record*, Record No. 15015; Department of Energy, 2015.

(4) Merki, D.; Fierro, S.; Vrubel, H.; Hu, X. Conducting MoS_2 Nanosheets as Catalysts for Hydrogen Evolution Reaction. *Chem. Sci.* **2011**, *2*, 1262−1267.

(5) Cao, Y. Roadmap and Direction toward High-Performance MoS2 Hydrogen Evolution Catalysts. *ACS Nano* **2021**, *15*, 11014−11039.

(6) Aliaga, J.; Vera, P.; Araya, J.; Ballesteros, L.; Urzúa, J.; Farías, M.; Paraguay-Delgado, F.; Alonso-Núñez, G.; González, G.; Benavente, E. Electrochemical Hydrogen Evolution over Hydrothermally Synthesized Re-Doped MoS2 Flower-Like Microspheres. *Molecules* **2019**, *24*, No. 4631.

(7) Xu, J.; Zhao, Z.; Wei, W.; Chang, G.; Xie, Z.; Guo, W.; Liu, D.; Qu, D.; Tang, H.; Li, J. Tuning the Intrinsic Activity and Electrochemical Surface Area of MoS 2 via Tiny Zn Doping: Toward an Efficient Hydrogen Evolution Reaction (HER) Catalyst. *Chem.—Eur. J.* **2021**, *27*, 15992−15999.

(8) Yang, Q.; Wang, Z.; Dong, L.; Zhao, W.; Jin, Y.; Fang, L.; Hu, B.; Dong, M. Activating MoS2 with Super-High Nitrogen-Doping Concentration as Efficient Catalyst for Hydrogen Evolution Reaction. *J. Phys. Chem. C* **2019**, *123*, 10917−10925.

(9) Li, G.; Chen, Z.; Li, Y.; Zhang, D.; Yang, W.; Liu, Y.; Cao, L. Engineering Substrate Interaction To Improve Hydrogen Evolution Catalysis of Monolayer MoS2 Films beyond Pt. *ACS Nano* **2020**, *14*, 1707−1714.

(10) Delmon, B. Influence of species diffusing at surfaces on reactions of solids and catalytic processes. *Solid State Ionics* **1997**, *101−103*, 655−660. International Symposium on the Reactivity of Solids.

(11) Tang, Q.; Jiang, D.-e. Mechanism of Hydrogen Evolution Reaction on 1T-MoS2 from First Principles. *ACS Catal.* **2016**, *6*, 4953−4961.

(12) Voiry, D.; Salehi, M.; Silva, R.; Fujita, T.; Chen, M.; Asefa, T.; Shenoy, V. B.; Eda, G.; Chhowalla, M. Conducting MoS2 Nanosheets as Catalysts for Hydrogen Evolution Reaction. *Nano Lett.* **2013**, *13*, 6222.

(13) Ruffman, C.; Gordon, C. K.; Skúlason, E.; Garden, A. L. Mechanisms and Potential-Dependent Energy Barriers for Hydrogen Evolution on Supported MoS2 Catalysts. *J. Phys. Chem. C* **2020**, *124*, 17015−17026.

(14) Benck, J. D.; Hellstern, T. R.; Kibsgaard, J.; Chakthranont, P.; Jaramillo, T. F. Catalyzing the Hydrogen Evolution Reaction (HER) with Molybdenum Sulfide Nanomaterials. *ACS Catal.* **2014**, *4*, 3957−3971.

(15) Wang, S.; Lu, A.; Zhong, C.-J. Hydrogen production from water electrolysis: role of catalysts. *Nano Convergence* **2021**, *8*, 1.

(16) Kuznetsov, V.; Lohstroh, W.; Rogalla, D.; Becker, H.-W.; Strunskus, T.; Nefedov, A.; Kovacevic, E.; Traeger, F.; Fouquet, P. Neutron spectroscopy study of the diffusivity of hydrogen in MoS2. *Phys. Chem. Chem. Phys.* **2021**, *23*, 7961−7973.

(17) Traeger, F.; Kauer, M.; Wöll, C.; Rogalla, D.; Becker, H.-W. Analysis of surface, subsurface, and bulk hydrogen in ZnO using nuclear reaction analysis. *Phys. Rev. B* **2011**, *84*, No. 075462.

(18) Sakurai, T.; Cardillo, M. J.; Hagstrum, H. D. Kinetics of the generation of atomic hydrogen and its adsorption on Si(110). *J. Vac. Sci. Technol.* **1977**, *14*, 397−399.

(19) Schulze, G.; Henzler, M. Adsorption of atomic hydrogen on clean cleaved silicon (111). *Surf. Sci.* **1983**, *124*, 336−350.

(20) Becker, H.-W.; Rogalla, D. In *Neutron Scattering and Other Nuclear Techniques for Hydrogen in Materials*; Fritzsche, H.; Huot, J.; Fruchart, D., Eds.; Springer International Publishing: Cham, 2016; pp 315−336.
(21) Klappenberger, F. Two-dimensional functional molecular nanoarchitectures − Complementary investigations with scanning tunneling microscopy and X-ray spectroscopy. *Prog. Surf. Sci.* **2014**, *89*, 1−55.
(22) Liu, T.; Temprano, I.; King, D. A.; Driver, S. M.; Jenkins, S. J. Epitaxial growth of few-layer MoS2(0001) on FeS2{100}. *Chem. Commun.* **2015**, *51*, 537−540.
(23) Powell, C.*NIST Electron Inelastic-Mean-Free-Path Database*, NIST Standard Reference Database 71; NIST, 1999.
(24) Shirley, D. A. High-Resolution X-ray Photoemission Spectrum of the Valence Bands of Gold. *Phys. Rev. B* **1972**, *5*, 4709−4714.
(25) Yeh, J.; Lindau, I. Atomic subshell photoionization cross sections and asymmetry parameters: 1 < Z < 103. *At. Data Nucl. Data Tables* **1985**, *32*, 1−155.
(26) Bée, M.*Quasielastic Neutron Scattering: Principles and Applications in Solid State Chemistry, Biology and Materials Science*; Adam Hilger: Bristol, 1988.
(27) Traeger, F.; Fouquet, P.; Koza, M. M.; Kuznetsov, V.Diffusion of Water and Hydrogen in MoS_2 (Single Crystal and Powder), 2020. https://doi.ill.fr/10.5291/ILL-DATA.7-05-509.
(28) Brochier, D.*Cryostat à température variable pour mesures neutroniques ou optiques*; Institute Max von Laue—Paul Langevin, 1977.
(29) Arnold, O.; Bilheux, J.; Borreguero, J.; Buts, A.; Campbell, S.; Chapon, L.; Doucet, M.; Draper, N.; Leal, R. F.; Gigg, M.; et al. Mantid − Data analysis and visualization package for neutron scattering and μ-SR experiments. *Nucl. Instrum. Methods Phys. Res., Sect. A* **2014**, *764*, 156−166.
(30) Sun, H.; Mumby, S. J.; Maple, J. R.; Hagler, A. T. An ab Initio CFF93 All-Atom Force Field for Polycarbonates. *J. Am. Chem. Soc.* **1994**, *116*, 2978−2987.
(31) Liu, J.; Zeng, J.; Zhu, C.; Miao, J.; Huang, Y.; Heinz, H. Interpretable molecular models for molybdenum disulfide and insight into selective peptide recognition. *Chem. Sci.* **2020**, *11*, 8708−8722.
(32) Dickinson, R. G.; Pauling, L. The Crystal Structure of Molybdenite. *J. Am. Chem. Soc.* **1923**, *45*, 1466−1471.
(33) Leimkuhler, B.; Noorizadeh, E.; Theil, F. A Gentle Stochastic Thermostat for Molecular Dynamics. *J. Stat. Phys.* **2009**, *135*, 261−277.
(34) Samoletov, A. A.; Dettmann, C. P.; Chaplain, M. A. J. Thermostats for "Slow" Configurational Modes. *J. Stat. Phys.* **2007**, *128*, 1321−1336.
(35) Ganta, D.; Sinha, S.; Haasch, R. T. 2-D Material Molybdenum Disulfide Analyzed by XPS. *Surf. Sci. Spectra* **2014**, *21*, 19−27.
(36) Choi, J.-G.; Thompson, L. XPS study of as-prepared and reduced molybdenum oxides. *Appl. Surf. Sci.* **1996**, *93*, 143−149.
(37) Gelius, U.; Hedén, P. F.; Hedman, J.; Lindberg, B. J.; Manne, R.; Nordberg, R.; Nordling, C.; Siegbahn, K. Molecular Spectroscopy by Means of ESCA III.Carbon compounds. *Phys. Scr.* **1970**, *2*, 70−80.
(38) Byskov, L. S.; Bollinger, M.; Nørskov, J. K.; Clausen, B. S.; Topsøe, H. Molecular aspects of the H2 activation on MoS2 based catalysts - the role of dynamic surface arrangements. *J. Mol. Catal. A: Chem.* **2000**, *163*, 117−122.
(39) An, Y.; Kuc, A.; Petkov, P.; Lozada-Hidalgo, M.; Heine, T. On the Chemistry and Diffusion of Hydrogen in the Interstitial Space of Layered Crystals h -BN, MoS 2, and Graphite. *Small* **2019**, *15*, No. 1901722.
(40) Bée, M. A physical insight into the elastic incoherent structure factor. *Phys. B* **1992**, *182*, 323−336.
(41) Volino, F.; Dianoux, A. Neutron incoherent scattering law for diffusion in a potential of spherical symmetry: general formalism and application to diffusion inside a sphere. *Mol. Phys.* **1980**, *41*, 271−279.
(42) Singwi, K. S.; Sjölander, A. Diffusive Motions in Water and Cold Neutron Scattering. *Phys. Rev.* **1960**, *119*, 863−871.
(43) Hall, P. L.; Ross, D. Incoherent neutron scattering functions for random jump diffusion in bounded and infinite media. *Mol. Phys.* **1981**, *42*, 673−682.
(44) Chudley, C. T.; Elliott, R. J. Neutron Scattering from a Liquid on a Jump Diffusion Model. *Proc. Phys. Soc.* **1961**, *77*, 353−361.
(45) Graham, A. P.; Menzel, A.; Toennies, J. P. Quasielastic helium atom scattering measurements of microscopic diffusional dynamics of H and D on the Pt(111) surface. *J. Chem. Phys.* **1999**, *111*, 1676−1685.

https://doi.org/10.1021/acs.jpcc.2c03848
J. Phys. Chem. C 2022, 126, 21667−21680